

Power-law expansion of the Universe from the bosonic Lorentzian type IIB matrix model

Yuta Ito,^a Jun Nishimura^{ab} and Asato Tsuchiya^c

^a*Department of Particle and Nuclear Physics,
Graduate University for Advanced Studies (SOKENDAI),
Tsukuba, Ibaraki 305-0801, Japan*

^b*High Energy Accelerator Research Organization (KEK),
Tsukuba, Ibaraki 305-0801, Japan*

^c*Department of Physics, Shizuoka University,
836 Ohya, Suruga-ku, Shizuoka 422-8529, Japan*

yito@post.kek.jp, jnishi@post.kek.jp, satsuch@ipc.shizuoka.ac.jp

ABSTRACT: Recent studies on the Lorentzian version of the type IIB matrix model show that (3+1)D expanding universe emerges dynamically from (9+1)D space-time predicted by superstring theory. Here we study a bosonic matrix model obtained by omitting the fermionic matrices. With the adopted simplification and the usage of a large-scale parallel computer, we are able to perform Monte Carlo calculations with matrix size up to $N = 512$, which is twenty times larger than that used previously for the studies of the original model. When the matrix size is larger than some critical value $N_c \simeq 110$, we find that (3+1)D expanding universe emerges dynamically with a clear large- N scaling property. Furthermore, at sufficiently late times, we observe a power-law behavior $t^{1/2}$ of the spatial extent with respect to time t , which is reminiscent of the expanding behavior of the Friedmann-Robertson-Walker universe in the radiation dominated era. We discuss possible implications of this result on the original model including fermionic matrices.

KEYWORDS: Matrix Models, 1/N Expansion.

Contents

1. Introduction	1
2. Brief review of the Lorentzian type IIB matrix model	3
3. The bosonic Lorentzian type IIB matrix model	6
4. Properties of the bosonic model for $N < N_c$	7
5. Properties of the bosonic model for $N \geq N_c$	8
6. Summary and discussions	12
A. Details of Monte Carlo simulation	13
B. Results for the (5+1)D version of the bosonic model	15

1. Introduction

Understanding how our universe began is a fascinating subject in theoretical physics. This is, of course, not so easy since one has to deal with quantum gravity near cosmic singularity, which appears in general relativity. As a promising way to describe quantum gravity, string theory has been studied for many years. However, as far as one applies perturbative string theory around a time dependent background, cosmic singularity cannot be resolved in general [1–4]. It is therefore necessary to study string theory in a nonperturbative background-independent fashion. As nonperturbative formulations of superstring/M theory, matrix models that can be obtained formally by dimensionally reducing 10D $\mathcal{N} = 1$ super Yang-Mills theory to $d = 0$ [5], $d = 1$ [6] and $d = 2$ [7] were proposed. As a closely related direction, ref. [8,9] proposes a conformal field theory, which is holographically dual to inflationary models.

The type IIB matrix model [5] is one of these proposals corresponding to the $d = 0$ case above. A peculiar feature of this model is that both space and time emerge dynamically from the matrix degrees of freedom. In this context, the idea of emergent gravity has been pursued [10–17] in gauge theories on non-commutative space that appear from the type IIB matrix model for a particular class of backgrounds [18–21]. There are also other proposals for the description of curved space-time in matrix models [22–24].

Until recently, the type IIB matrix model was studied after the “Wick rotation” [25–38] since the partition function of the Euclidean model obtained in this way is shown to be

finite [39,40]. However, the Euclidean model is clearly not suitable for studying the real-time dynamics since the time coordinate is treated as purely imaginary due to the “Wick rotation”. Moreover, it is known that the Wick rotation is more subtle in quantum gravity than in quantum field theories at the nonperturbative level (See, for instance, refs. [41,42]). In fact, according to a recent study of the Euclidean model using the Gaussian expansion method, the emergent space-time seems to have only three dimensions [43].

On the other hand, the Lorentzian version of the type IIB matrix model has been studied for the first time in ref. [44]. Unlike the Euclidean version, one has to introduce infrared cutoffs in the temporal and spatial directions to make the partition function finite. Despite this subtlety, the time-evolution of the “universe” was extracted from the matrix configurations generated by Monte Carlo simulation, and a large- N scaling behavior was observed with the matrix size $N \leq 16$. Quite remarkably, the $SO(9)$ rotational symmetry of the 9D space turned out to be spontaneously broken down to $SO(3)$ at some critical time, after which only three out of the nine spatial directions start to expand.

In order to see what happens at later times in this model, one needs to increase the matrix size, which makes the Monte Carlo simulation more and more time-consuming. As an alternative approach, one can use the classical approximation [45–49] to investigate possible behaviors at late times since each term in the action becomes large as the expansion of the “universe” proceeds. A general prescription to construct solutions to the classical equations of motion was given in ref. [46]. One can actually construct classical solutions corresponding to an expanding (3+1)D universe, which naturally solve the cosmological constant problem [46]. As a closely related progress, it was found that matrix configurations with intersecting fuzzy spheres in the extra dimensions can accommodate the standard model fermions [50–56].

In fact, it is known that the classical equations of motion of the matrix model have infinitely many solutions [46]. Therefore, in order to determine which classical solution is actually realized at late times, we need to study the time-evolution of the “universe” at least for a sufficiently long time by performing Monte Carlo simulation. To that end, we previously studied a simplified model that describes the early time behaviors of the original model [57]. With the matrix size $N \leq 64$, we observed a clear exponentially expanding behavior, which is reminiscent of the inflation. Monte Carlo studies of the original model with $N = 24$ [58] yielded results consistent with this observation.

In this paper we study a bosonic model, which can be obtained by simply omitting the fermionic matrices. This simplification and the usage of a large-scale parallel computer enable us to perform Monte Carlo simulation with the matrix size up to $N = 512$. Unlike the original model, the eigenvalue distribution of the temporal matrix turns out to have a finite extent without introducing a cutoff in the temporal direction. The extent of the eigenvalue distribution is independent of N for $N < N_c \simeq 110$, but it increases with N for $N \geq N_c$. We find that the properties of the model changes drastically at the critical $N = N_c$. For $N < N_c$, the dominant matrix configurations do not allow extraction of a well-defined time-evolution. For $N \geq N_c$, on the other hand, we can extract a meaningful time-evolution, which shows that the $SO(9)$ rotational symmetry is broken spontaneously down to $SO(3)$ symmetry at some point in time similarly to the original model. The large-

N scaling behavior is clearly observed. The expanding behavior of the spatial extent can be fitted by an exponential function only for a rather short period, and after that it becomes a power-law $t^{1/2}$ with respect to time t . The latter behavior coincides with the expanding behavior of the Friedmann-Robertson-Walker universe in the radiation dominated era. From these results, we speculate that the exponential expansion of the space in the original model suggested in the previous works actually terminates at some point in time and turns into a power law similarly to the bosonic model. This would imply that the number of e-foldings is determined dynamically in the Lorentzian type IIB matrix model.

The rest of this paper is organized as follows. In section 2 we briefly review some important properties of the Lorentzian type IIB matrix model. In section 3 we define the bosonic model we study in this paper, and discuss the existence of the critical N , at which the properties of the model change drastically. In sections 4 and 5 we discuss in detail the properties of the model below and above N_c , respectively. Section 6 is devoted to a summary and discussions. In Appendix A we give the details of our simulation. In Appendix B we present our results for the (5+1)D version of the bosonic model.

2. Brief review of the Lorentzian type IIB matrix model

The action of the Lorentzian type IIB matrix model is given by [5]

$$S = S_b + S_f , \quad (2.1)$$

$$S_b = \frac{1}{4g^2} \text{Tr} ([A_\mu, A_\nu] [A^\mu, A^\nu]) , \quad (2.2)$$

$$S_f = -\frac{1}{2g^2} \text{Tr} \left(\Psi_\alpha (\mathcal{C}\Gamma^\mu)_{\alpha\beta} [A_\mu, \Psi_\beta] \right) , \quad (2.3)$$

where the bosonic $N \times N$ matrices A_μ ($\mu = 0, \dots, 9$) and the fermionic matrices Ψ_α ($\alpha = 1, \dots, 16$) are both traceless and Hermitian. Γ^μ are 10D gamma-matrices after the Weyl projection and \mathcal{C} is the charge conjugation matrix. The ‘‘coupling constant’’ g is merely a scale parameter in this model since it can be absorbed by rescaling A_μ and Ψ appropriately. The indices μ and ν are contracted using the Lorentzian metric $\eta_{\mu\nu} = \text{diag}(-1, 1, \dots, 1)$. The Euclidean version can be obtained by making the ‘‘Wick rotation’’ $A_0 = iA_{10}$, where A_{10} is supposed to be Hermitian.

The partition function for the Lorentzian version is proposed in ref. [44] as

$$Z = \int dA d\Psi e^{iS} \quad (2.4)$$

with the action (2.1). The ‘‘ i ’’ in front of the action is motivated from the fact that the string world-sheet metric should also have a Lorentzian signature. By integrating out the fermionic matrices, we obtain the Pfaffian

$$\int d\Psi e^{iS_f} = \text{Pf} \mathcal{M}(A) , \quad (2.5)$$

which is real unlike in the Euclidean case [38]. Note also that the bosonic action (2.2) can be written as

$$S_b = \frac{1}{4g^2} \text{Tr} (F_{\mu\nu} F^{\mu\nu}) = \frac{1}{4g^2} \left\{ -2\text{Tr} (F_{0i})^2 + \text{Tr} (F_{ij})^2 \right\} , \quad (2.6)$$

where we have introduced the Hermitian matrices $F_{\mu\nu} = i[A_\mu, A_\nu]$. Since the two terms in the last expression have opposite signs, S_b is not positive semi-definite, and it is not bounded from below.

In order to make the partition function (2.4) finite, one needs to introduce infrared cutoffs in both the temporal and spatial directions, for instance, as [44]

$$\frac{1}{N} \text{Tr} (A_0)^2 \leq \kappa \frac{1}{N} \text{Tr} (A_i)^2 , \quad (2.7)$$

$$\frac{1}{N} \text{Tr} (A_i)^2 \leq \Lambda^2 . \quad (2.8)$$

It was found that the two parameters κ and Λ can be removed in the large- N limit in such a way that physical quantities scale [44]. Therefore the resulting theory can be characterized by a single scale parameter.

In the present work, it will be important to understand the reason why we need to introduce the cutoff (2.7) in the temporal direction. Note first that one can use the $SU(N)$ symmetry of the model to bring the temporal matrix A_0 into the diagonal form

$$A_0 = \text{diag} (\alpha_1, \dots, \alpha_N) , \quad \text{where } \alpha_1 < \dots < \alpha_N . \quad (2.9)$$

By ‘‘fixing the gauge’’ in this way, we can rewrite the partition function (2.4) as

$$Z = \int \prod_{a=1}^N d\alpha_a \Delta(\alpha)^2 \int dA_i d\Psi e^{iS} , \quad (2.10)$$

$$\Delta(\alpha) \equiv \prod_{a>b}^N (\alpha_a - \alpha_b) , \quad (2.11)$$

where $\Delta(\alpha)$ is the van der Monde determinant. The factor $\Delta(\alpha)^2$ in (2.10) appears from the Fadeev-Popov procedure for the gauge fixing, and it acts as a repulsive potential between the eigenvalues α_i of A_0 . Here we consider a situation in which the eigenvalues of A_0 are well separated from each other. Then the action $S = S_b + S_f$ can be expanded as

$$S_b = -\frac{1}{2g^2} (\alpha_a - \alpha_b)^2 |(A_i)_{ab}|^2 + \dots , \quad (2.12)$$

$$S_f = -\frac{1}{2g^2} (\Psi_\alpha)_{ba} (\alpha_a - \alpha_b) (C\Gamma^\mu)_{\alpha\beta} (\Psi_\beta)_{ab} + \dots , \quad (2.13)$$

omitting the subleading terms for large $|\alpha_a - \alpha_b|$. Integrating out A_i at one loop neglecting the zero modes corresponding to diagonal elements, we obtain $\Delta(\alpha)^{-18}$. On the other hand, integrating out Ψ_α at one loop similarly, we obtain $\Delta(\alpha)^{16}$. Thus we find that the potential between α_i is canceled exactly at the one-loop level. This is actually a consequence of supersymmetry [5] of the model (2.4). Owing to this property, the eigenvalue distribution of A_0 extends to infinity even for finite N if the cutoff (2.7) were absent.

In fact, after some manipulation and rescaling of A_μ , we can rewrite the partition function (2.4) as [44] (See Appendix A of ref. [57] for a refined argument.)

$$Z = \int dA \text{Pf} \mathcal{M}(A) \delta \left(\frac{1}{N} \text{Tr} (F_{\mu\nu} F^{\mu\nu}) \right) \delta \left(\frac{1}{N} \text{Tr} (A_i)^2 - 1 \right) \theta \left(\kappa - \frac{1}{N} \text{Tr} (A_0)^2 \right) ,$$

$$\begin{aligned}
&= \int \prod_{a=1}^N d\alpha_a \prod_{i=1}^d dA_i \Delta^2(\alpha) \text{Pf}\mathcal{M}(A) \delta\left(\frac{1}{N} \text{Tr}(F_{\mu\nu} F^{\mu\nu})\right) \\
&\quad \times \delta\left(\frac{1}{N} \text{Tr}(A_i)^2 - 1\right) \theta\left(\kappa - \frac{1}{N} \text{Tr}(A_0)^2\right) , \tag{2.14}
\end{aligned}$$

where $\theta(x)$ is the Heaviside step function. This form allows us to performing Monte Carlo simulation of the Lorentzian model without the sign problem unlike the Euclidean model.¹

It turns out that one can extract a time-evolution from configurations generated by simulating (2.14). A crucial observation is that the spatial matrices A_i have a band-diagonal structure in the $\text{SU}(N)$ basis in which A_0 has the diagonal form (2.9). More precisely, there exists some integer n such that the elements of spatial matrices $(A_i)_{ab}$ for $|a-b| > n$ are much smaller than those for $|a-b| \leq n$. Based on this observation, we may naturally consider $n \times n$ matrices

$$(\bar{A}_i)_{IJ}(t) \equiv (A_i)_{\nu+I, \nu+J} , \tag{2.15}$$

as representing the state of the universe at time t , where $I, J = 1, \dots, n$ and $\nu = 0, 1, \dots, N-n$. The time t in (2.15) is defined by

$$t = \frac{1}{n} \sum_{I=1}^n \alpha_{\nu+I} \tag{2.16}$$

corresponding to the $n \times n$ matrices \bar{A}_i . For example, we can define the extent of space at time t as

$$R^2(t) = \left\langle \frac{1}{n} \text{tr} \sum_i (\bar{A}_i(t))^2 \right\rangle , \tag{2.17}$$

where the symbol tr represents a trace over the $n \times n$ block. We also define the ‘‘moment of inertia tensor’’

$$T_{ij}(t) = \frac{1}{n} \text{tr} (\bar{A}_i(t) \bar{A}_j(t)) , \tag{2.18}$$

which is a 9×9 real symmetric matrix. The eigenvalues of $T_{ij}(t)$, which we denote by $\lambda_i(t)$ with the order

$$\lambda_1(t) > \lambda_2(t) > \dots > \lambda_9(t) , \tag{2.19}$$

represent the spatial extent in each of the nine directions at time t . Note that the expectation values $\langle \lambda_i(t) \rangle$ tend to be equal in the large- N limit if the $\text{SO}(9)$ symmetry is not spontaneously broken. This is the case at early times of the time-evolution. After a critical time t_c , however, we find that three largest eigenvalues $\langle \lambda_i(t) \rangle$ ($i = 1, 2, 3$) become significantly larger than the others, which implies that the $\text{SO}(9)$ symmetry is spontaneously broken down to $\text{SO}(3)$.

It would be interesting to study a long time-evolution of the model and see how the expansion of space proceeds. This requires very large matrices, which makes the simulation unfeasible. In the previous work [57], we studied a simplified model, in which the Pfaffian

¹Strictly speaking, the Pfaffian $\text{Pf}\mathcal{M}$ in (2.14) can change its sign, but it turned out that configurations with positive Pfaffian dominate at large N .

is replaced by the one-loop contribution $\Delta(\alpha)^{16}$ mentioned above. This replacement is expected to be valid at early times, where the expansion of space has not proceeded much and the leading term in (2.13) is indeed dominant. According to the argument below (2.13), the potential between the eigenvalues of A_0 is canceled at one loop and hence the cutoff (2.7) in the temporal direction is needed in this simplified model as well as in the original model. On the other hand, this simplified model can be simulated with much less effort than the original model.² In ref. [57] the (5+1)D version of the simplified model was studied with the matrix size $N \leq 64$, and the $SO(5)$ symmetry was found to be broken spontaneously down to $SO(3)$ at some point in time similarly to the original model. Moreover, the expanding behavior of the 3D space turned out to be exponential,³ and no tendencies of slowing down were observed within the scaling region. Analogous behaviors were also confirmed for the (9+1)D version of the simplified model. In the original model, on the other hand, the subleading term in the fermionic action (2.13) becomes important at late times as the expansion proceeds, and hence it can affect the expanding behavior.

3. The bosonic Lorentzian type IIB matrix model

In this paper we study a bosonic model in which the fermionic matrices are simply omitted. The partition function is given by

$$Z = \int dA e^{iS_b} . \quad (3.1)$$

In section 2 we reviewed an argument for the necessity of the temporal cutoff in the original model and the simplified model for early times. In the present case of the bosonic model (3.1), the same argument implies that there is no need to introduce the temporal cutoff (2.7), and that we only need a cutoff (2.8) in the spatial direction. Corresponding to (2.14), we can study the bosonic Lorentzian type IIB matrix model by simulating

$$Z = \int dA \delta \left(\frac{1}{N} \text{Tr} (F_{\mu\nu} F^{\mu\nu}) \right) \delta \left(\frac{1}{N} \text{Tr} (A_i)^2 - 1 \right) \quad (3.2)$$

$$= \int \prod_{a=1}^N d\alpha_a \prod_{i=1}^d dA_i \Delta^2(\alpha) \delta \left(\frac{1}{N} \text{Tr} (F_{\mu\nu} F^{\mu\nu}) \right) \delta \left(\frac{1}{N} \text{Tr} (A_i)^2 - 1 \right) , \quad (3.3)$$

which requires computational efforts comparable to the simplified model for early times reviewed in the previous section. We have used a large-scale parallel computer to simulate the model (3.3) with the matrix size up to $N = 512$, which enables us to investigate a long time-evolution. See Appendix A for the details of the simulation.

We measure the quantity $\langle \frac{1}{N} \text{Tr} (A_0)^2 \rangle$, which represents the extent of the eigenvalue distribution of A_0 . As we mentioned above, this quantity turns out to be finite in the model

²In order to make one trajectory in the Hybrid Monte Carlo algorithm, the original model requires $O(N^5)$ arithmetic operations, whereas the simplified model requires only $O(N^3)$ arithmetic operations. The reason for this is that the number of iterations required for the convergence of the conjugate gradient method used to implement the effects of fermions grows as $O(N^2)$.

³This behavior is also confirmed with smaller matrix size $N \leq 32$ with the aid of a renormalization group method developed in the same paper [57].

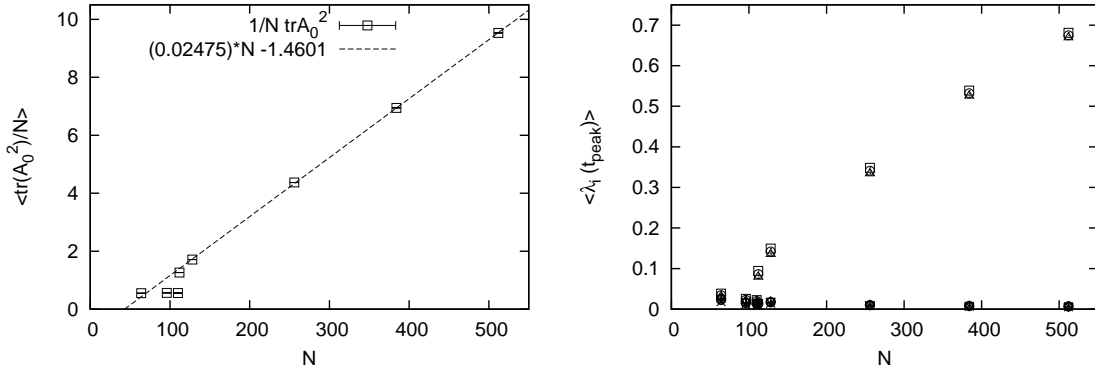


Figure 1: (Left) The extent $\langle \frac{1}{N} \text{Tr}(A_0)^2 \rangle$ of the eigenvalue distribution of A_0 is plotted against N . (Right) The expectation values $\lambda_i(t)$ of the nine eigenvalues of $T_{ij}(t)$ at $t = t_{\text{peak}}$ are plotted against N . For $N < N_c = 112$, the nine eigenvalues are close to each other, whereas for $N \geq N_c$, three out of the nine eigenvalues become much larger than the others.

(3.3) although we do not introduce a cutoff in the temporal direction such as (2.7). In Fig. 1 (Left) we plot the results against N . At small N , it is almost independent of N . However, for $N \geq N_c = 112$, it begins to increase linearly with N . Figure 1 (Right) shows the N dependence of the expectation values $\langle \lambda_i(t) \rangle$ of the nine eigenvalues of $T_{ij}(t)$ evaluated at $t = t_{\text{peak}}$, where $R^2(t)$ becomes maximum.⁴ For small N , there is no significant gap between the nine eigenvalues, whereas for $N \geq N_c$, we observe a big gap between $\langle \lambda_3(t_{\text{peak}}) \rangle$ and $\langle \lambda_4(t_{\text{peak}}) \rangle$. We will see in section 5 that the $\text{SO}(9)$ symmetry is broken down to $\text{SO}(3)$ after a critical time similarly to the original Lorentzian type IIB matrix model.

4. Properties of the bosonic model for $N < N_c$

In this section we discuss the properties of the bosonic model for $N < N_c$. In order to extract the time-evolution, we need to determine the block size n to be used in eq. (2.15). In Fig. 2 (Left) we plot the magnitude of the off-diagonal elements of A_i against the time separation $\alpha_a - \alpha_b$ for $N = 110$. The origin in the horizontal axis corresponds to the diagonal elements. We observe a nice scaling behavior for all the matrix elements. However, the magnitude falls off rather smoothly as one goes in the off-diagonal direction, which means that the dominant matrix configurations do not have a band-diagonal structure.

In this situation, we cannot naturally define the block matrices (2.15) representing the state at each time and hence the notion of time-evolution becomes obscure. Let us nevertheless try to extract the “time-evolution” using $n = 14$ as the block size, which is the value obtained for $N = N_c = 112$ in the way described in the next section. In Fig. 2 (Right) we plot the expectation values $\langle \lambda_i(t) \rangle$ for $N = 110$. It turns out that there is only little t -dependence, and there is no clear gap between the eigenvalues for all t .

⁴In order to define $R^2(t)$ and $T_{ij}(t)$, we have to specify the block size n to be used in eq. (2.15). See sections 4 and 5 for the actual values of n used to obtain the results in Fig. 1 (Right).

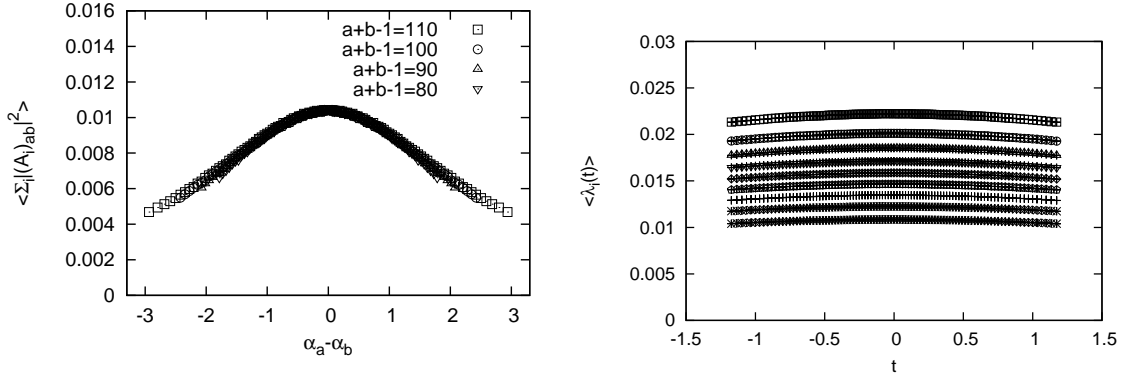


Figure 2: (Left) The magnitude $\sum_i |(A_i)_{ab}|^2$ of the off-diagonal elements of A_i is plotted against the time separation $\alpha_a - \alpha_b$ for $N = 110$. (Right) The expectation values $\langle \lambda_i(t) \rangle$ of the nine eigenvalues of $T_{ij}(t)$ are plotted against t for $N = 110$. The block size is chosen to be $n = 14$.

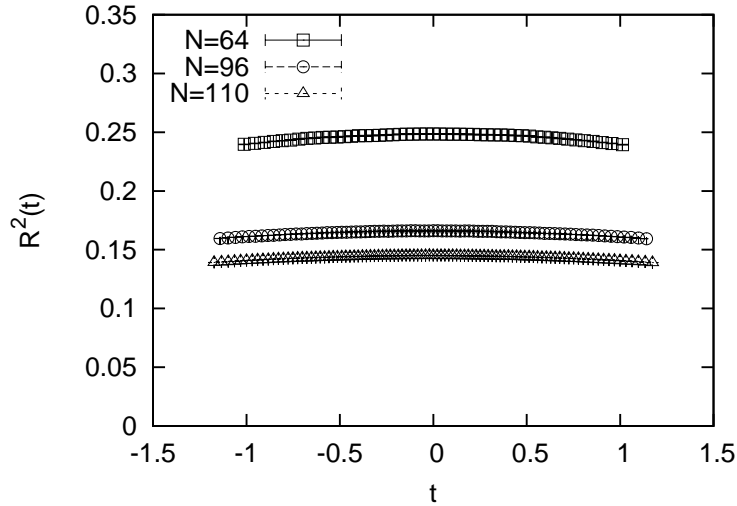


Figure 3: The extent of space $R^2(t)$ is plotted against t for $N = 64, 96$ and 110 . The block size is chosen to be $n = 14$ for all N .

The situation for smaller N is similar to the $N = 110$ case. In Fig. 3 we plot the extent of space $R^2(t)$ as a function of t for $N = 64, 96$ and 110 obtained with the same block size $n = 14$. The dependence on N turns out to be modest.

5. Properties of the bosonic model for $N \geq N_c$

In this section we study the properties of the bosonic model for $N \geq N_c$. In Fig. 4 (Left) we plot the magnitude of the off-diagonal elements of A_i for $N = 128$. We find that the magnitude decreases rapidly as one goes away from diagonal elements. Moreover, the magnitude scales only for sufficiently large $|\alpha_a - \alpha_b|$. From this observation, we identify the block size n as the number of points in the region where the off-diagonal elements do

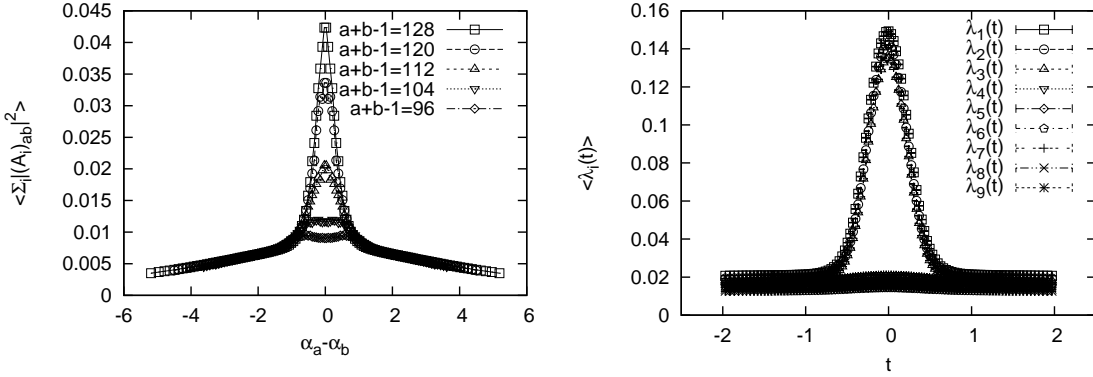


Figure 4: (Left) The magnitude $\sum_i |(A_i)_{ab}|^2$ of the off-diagonal elements of A_i is plotted against the time separation $\alpha_a - \alpha_b$ for $N = 128$. The scaling is observed only for sufficiently large $|\alpha_a - \alpha_b|$. (Right) The expectation values $\langle \lambda_i(t) \rangle$ of the nine eigenvalues of $T_{ij}(t)$ are plotted against t for $N = 128$ with the block size $n = 20$.

not scale. (In the present $N = 128$ case, we obtain $n = 20$. See below for more detail.) Using the block size n determined in this way, we can obtain the time-evolution. In Fig. 4 (Right) we plot the expectation values $\langle \lambda_i(t) \rangle$ for $N = 128$. In contrast to the situation for $N < N_c$, we observe the spontaneous symmetry breaking from $SO(9)$ to $SO(3)$ at a critical time t_c similarly to the original Lorentzian type IIB matrix model.⁵

In order to study the large- N scaling property, we perform simulation for $N = 256, 384, 512$ as well. In Fig. 5 (Top-Left) we zoom up the region near the origin in Fig. 4 (Left). From this figure, we determine the block size for $N = 128$ to be $n = 20$. Similarly, from the other figures in Fig. 5, we determine the block size for $N = 256, N = 384$ and 512 to be $n = 24, n = 28$ and 32 , respectively.

The definition of the critical time t_c is ambiguous at finite N . See Fig. 6 (Left), where we plot the expectation values $\langle \lambda_i(t) \rangle$ of the eigenvalues of $T_{ij}(t)$ against t for $N = 512$. Note first that the appearance of a gap between $\langle \lambda_3(t) \rangle$ and $\langle \lambda_4(t) \rangle$ signals the spontaneous symmetry breaking of $SO(9)$ to $SO(3)$. Let us therefore define the separation $d_j(t) = \langle \lambda_j(t) \rangle - \langle \lambda_{j+1}(t) \rangle$. Then we find that the symmetric phase can be characterized by $d_1(t) > d_2(t) > \dots > d_8(t)$, while in the broken phase we find $d_2(t) < d_3(t)$. Therefore we may define the critical time t_c by the largest value of t' such that $d_1(t) > d_2(t) > \dots > d_8(t)$ holds for $t \leq t'$. For instance, the critical time t_c obtained in this way for $N = 512$ from Fig. 6 (Left) is $t_c = -0.76559(7)$. Similarly we obtain $t_c = -0.76930(7)$ for $N = 384$. Applying the same procedure to smaller N , we find that the large- N scaling behavior in Fig. 6 (Right) becomes less clear due to finite N effects. We absorb these finite N effects by adjusting the value of t_c slightly⁶ from the one determined from the above procedure.

⁵The fact that the spatial dimensionality after the spontaneous symmetry breaking turned out to be the same as in the original model is understandable from the view point of the mechanism suggested in ref. [44], which involves only the boson part of the action.

⁶For $N = 256$, we shift by two data points and use $t_c = -0.82166(6)$ instead of $t_c = -0.76987(6)$. Similarly, for $N = 128$, we shift by four data points and use $t_c = -0.89472(7)$ instead of $t_c = -0.75798(7)$.

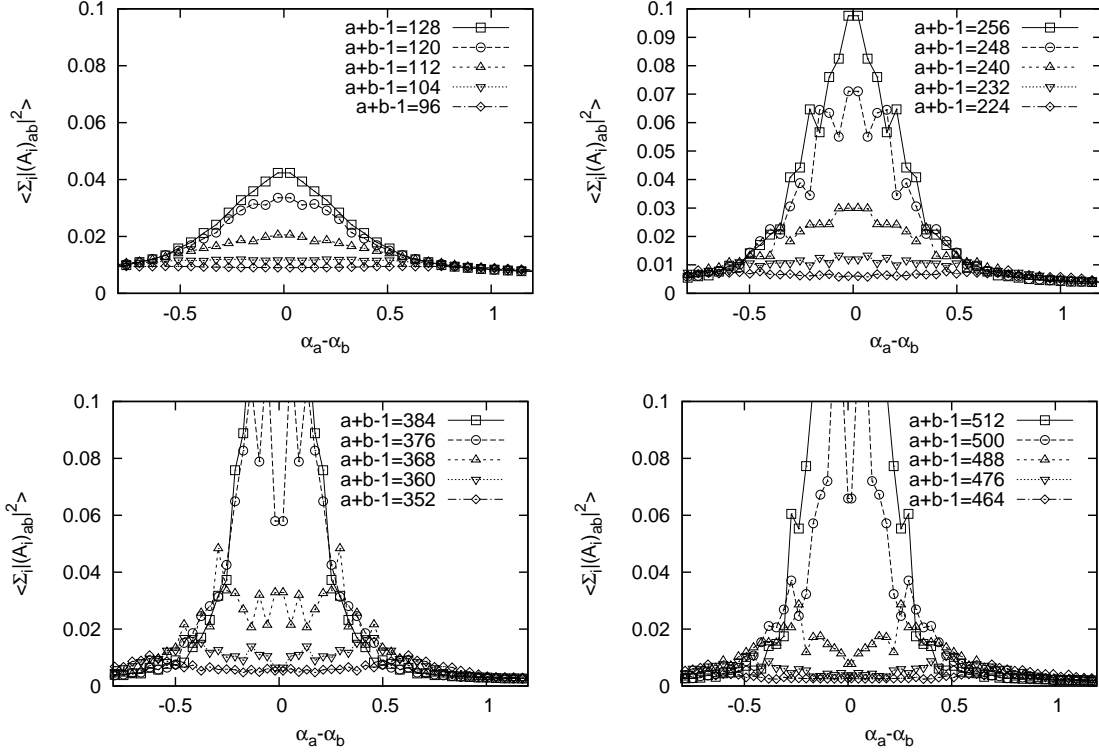


Figure 5: (Top-Left) The zoom up of the region near the origin in Fig. 4 (Left). We find 20 points in the region in which the scaling behavior is violated. Analogous plots for $N = 256$, $N = 384$, $N = 512$ are shown in the other panels, where we find 24, 28, 32 points in the non-scaling region, respectively.

As is proposed in the original Lorentzian type IIB matrix model [44], we use the extent of space $R(t_c)$ at the critical time to fix the scale. Explicit values of $R(t_c)$ are given in table 1 together with the block size n and the critical time t_c for each N .

In Fig. 6 (Right) the extent of space $R^2(t)$ is plotted against t . The large- N scaling behavior is observed by shifting the time coordinate so that the critical time comes to the origin and by plotting dimensionful quantities in units of $R(t_c)$. The observed large- N scaling shows that the theory one obtains in the large- N limit is characterized by one scale parameter $R(t_c)$ and it does not contain any dimensionless parameters.

It turns out that the behavior of $R^2(t)$ at $t > t_c$ can be fitted to an exponential function only for a finite range. At later times, it can be fitted well by a straight line, which corresponds to the power-law expansion

$$R(t) \propto t^{1/2} . \quad (5.1)$$

Note that this behavior is observed within the scaling region, which implies that the suggested power law persists in the large- N limit at least for some time region. In Appendix B we present the results for the (5+1)D version of the bosonic type IIB matrix model. While

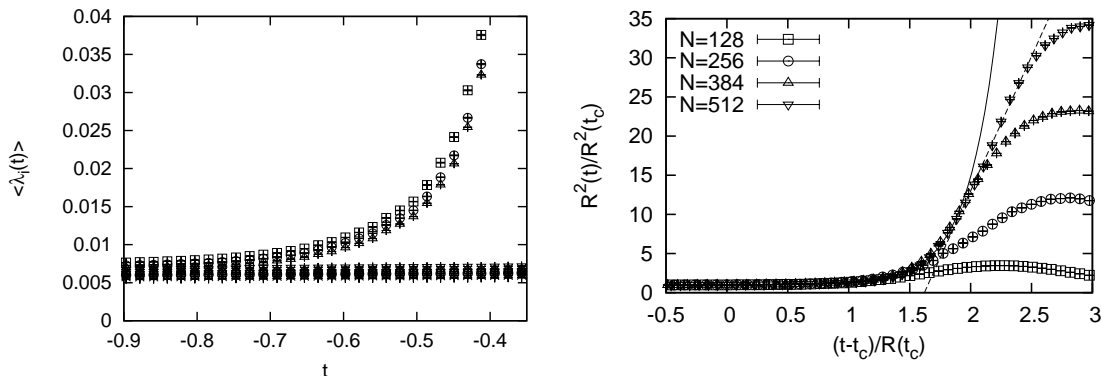


Figure 6: (Left) The expectation values $\langle \lambda_i(t) \rangle$ of the nine eigenvalues of $T_{ij}(t)$ are plotted against t for $N = 512$ with the block size $n = 32$. (Right) The extent of space $R^2(t)$ normalized by $R^2(t_c)$ is plotted against $x = (t - t_c)/R(t_c)$ for $N = 128, 256, 384$ and 512 . See table 1 for the values of the block size n , the critical time t_c and the extent of space $R(t_c)$ at the critical time, which are used to make this plot. The solid line is a fit of the $N = 512$ data to $R^2(t)/R^2(t_c) = a + (1 - a)\exp(bt)$ for $1.0 \leq x \leq 1.85$, which gives $a = 0.9957(5)$ and $b = 4.03(7)$. The dashed line is a fit of the $N = 512$ data to $R^2(t)/R^2(t_c) = cx + d$ for $1.85 \leq x \leq 2.5$, which gives $c = 34.3(6)$ and $d = -55(1)$.

we observe qualitatively the same behaviors, there are also some interesting quantitative differences.

In order to understand the observed large- N scaling further, we investigate how the continuum limit and the infinite volume limit in the temporal direction are achieved in the large- N limit. Here we restrict ourselves to $N \geq 256$ since $N = 128$ is too close to the critical value $N_c = 112$. As the “lattice spacing” in the temporal direction, we consider the separation of data points in Fig. 6 (Right) in the horizontal direction. This quantity is actually t -dependent, and it can be defined more explicitly as $\frac{\delta t}{R(t_c)}$, where δt is the difference of (2.16) between adjacent blocks. In Fig. 7 (Left) we plot this t -dependent “lattice spacing”, choosing the horizontal axis to be the same as in Fig. 6 (Right). We find clear tendency that the “lattice spacing” at the same point on the horizontal axis decreases as N increases. As the “volume” in the temporal direction, we define

$$\Delta \equiv \frac{(t_{\text{peak}} - t_c)}{R(t_c)}. \quad (5.2)$$

Using this quantity, we can also define an average “lattice spacing” $\varepsilon = \Delta/\nu$, where ν is the number of data points within the region $[t_c, t_{\text{peak}}]$. The values of ε and Δ obtained for each N are given in table 1. We find that the average “lattice spacing” ε decreases and the “volume” increases as N becomes large. In Fig. 7 (Right) we plot ε and Δ against N in the log scale. The straight lines represent fits to the power-law behaviors, although the behaviors may be subject to a qualitative change at larger N . In particular, it is an interesting dynamical question whether $\Delta \rightarrow \infty$ or $\Delta \rightarrow \text{const.}$ in the large- N limit. In the former case, the expansion of space continues forever, since the time t_{peak} at the peak cannot be reached within a finite time. In the latter case, on the other hand, the space

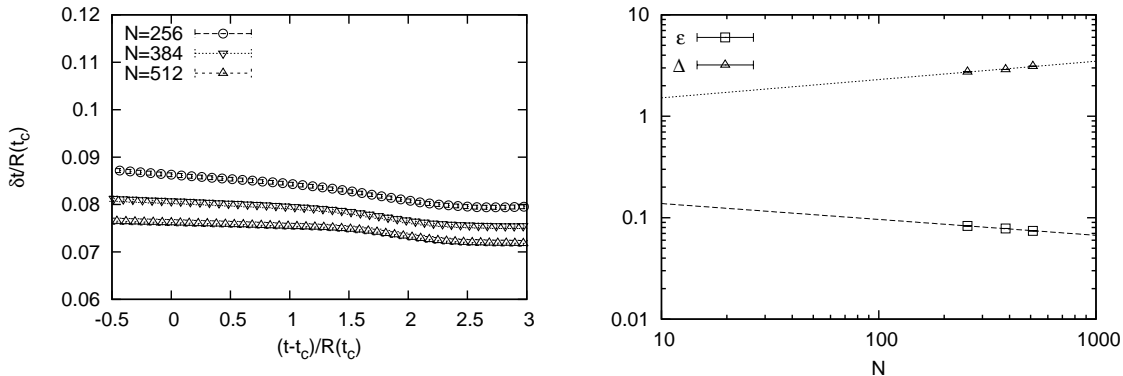


Figure 7: (Left) The “lattice spacing” $\frac{\delta t}{R(t_c)}$ is plotted against $(t - t_c)/R(t_c)$. (Right) The average “lattice spacing” ϵ and the “volume” in the temporal direction Δ is plotted against N in the log scale. The straight lines represent fits to the power-law behaviors $\epsilon = a N^{-p}$, where $a = 0.20(1)$, $p = 0.16(1)$ and $\Delta = b N^q$, where $b = 1.0(2)$, $q = 0.18(3)$.

N	n	t_c	$R(t_c)$	ϵ	Δ
128	20	-0.89472(7)	0.39270(2)	—	—
256	24	-0.82166(6)	0.30045(3)	0.08297(2)	2.7380(7)
384	28	-0.76930(7)	0.26580(3)	0.07823(2)	2.8943(6)
512	32	-0.76559(7)	0.24578(3)	0.07417(2)	3.1150(7)

Table 1: The block size n , the critical time t_c and the extent of space $R(t_c)$ at the critical time, which are used to make the plot in Fig. 6 (Right). We also present the explicit values of the average “lattice spacing” ϵ and the “volume” Δ in the temporal direction, which are plotted in Fig. 7 (Right).

stops expanding in a finite time and starts to shrink. By addressing this issue in the original model, one can, in principle, predict the fate of our Universe.

6. Summary and discussions

In this paper we have studied a bosonic model, which can be obtained from the Lorentzian type IIB matrix model by omitting the fermionic matrices. Due to the attractive potential between the eigenvalues of A_0 arising from integrating out the spatial matrices at one loop, the eigenvalue distribution of A_0 has a finite extent even if one does not introduce the temporal cutoff (2.7). In the original model, this attractive potential is canceled by the repulsive potential arising from integrating out the fermionic matrices at one loop and from the van der Monde determinant. (The simplified model for early times studied in ref. [57] has the same feature since the Pfaffian is replaced by the one-loop contribution.) Therefore, one would naively think that supersymmetry is playing an important role in the properties of the model that enable the extraction of a sensible time-evolution.

Indeed for $N < N_c$, we observe that the extent of the eigenvalue distribution of A_0 is almost independent of N , and the dominant matrix configurations do not allow the

extraction of a sensible time-evolution. However, for $N \geq N_c$, we find that the extent of the eigenvalue distribution of A_0 grows linearly in N , and a sensible time-evolution can be extracted. We find that the $SO(9)$ symmetry is spontaneously broken down to $SO(3)$ at some critical time similarly to the original model [44]. The quantity such as $R(t)$ shows a clear large- N scaling behavior. The growth of $R(t) \propto t^{1/2}$ at late times is reminiscent of the behavior of the Friedmann-Robertson-Walker universe in the radiation dominated era.

Let us recall that in the simplified model for early times, the growth of $R(t)$ was observed to be exponential [57]. In that model, only the first term in (2.13) was used to represent the effect of fermionic matrices. We consider that the exponential expansion occurs also in the original model at early times as is suggested by direct Monte Carlo studies up to $N \leq 24$ [58]. At late times, however, the subleading term in (2.13) becomes important due to the expansion of space, and that would affect the expanding behavior. Note that the repulsive potential for the eigenvalues of A_0 is obtained from integrating out the fermionic matrices without the subleading term. Therefore one of the effects of the subleading term would be to make the repulsive potential less effective. Considering that the bosonic model mimics such a situation, we speculate that the exponential expansion in the original model changes into a power-law expansion at some point in time, where the subleading term in (2.13) becomes important. According to this scenario, the number of e-foldings is determined dynamically in the Lorentzian type IIB matrix model. It would be interesting to confirm the transition directly by simulating the original model. An attempt in doing this with a systematic approximation is in progress.

Acknowledgements

We would like to thank K. Anagnostopoulos, T. Azuma, H. Kawai and S.-W. Kim for discussions. This research used computational resources of the K computer of the HPCI system provided by the AICS through the HPCI System Research Project (Project ID : hp130063). The supercomputer FX10 at University of Tokyo has been used in developing our code for parallel computing. Computation for the (5+1)D matrix model discussed in the Appendix B was carried out mostly on PC clusters at KEK. The work of Y. I. is supported by Grant-in-Aid for JSPS fellows. The work of J. N. and A. T. is supported by Grant-in-Aid for Scientific Research (No. 24540264, 15K05046 and 23244057) from JSPS.

A. Details of Monte Carlo simulation

In this section we give the details on how we perform Monte Carlo simulation of the bosonic model (3.3).

First the delta functions in (3.3) are replaced by Gaussian potentials as

$$V_{\text{pot}} = \frac{1}{2}\gamma_C \left(\frac{1}{N} \text{Tr}(F_{\mu\nu} F^{\mu\nu}) \right)^2 + \frac{1}{2}\gamma_L \left(\frac{1}{N} \text{Tr}(A_i)^2 - 1 \right)^2, \quad (\text{A.1})$$

where the coefficients γ_C and γ_L are taken large enough to fix each observable to the specified value. The values used in actual simulation are given in table 2.

Another important issue we have to take care of is the spontaneous breaking of the shift symmetry $A_0 \mapsto A_0 + \alpha \mathbf{1}$. For instance, let us consider calculating the expectation value $R^2(t)$ defined in (2.17). The peak of this quantity measured for each configuration fluctuates considerably. This reflects the ambiguity in choosing the origin of the time coordinate, and we should fix it before taking the ensemble average. Here we fix it by introducing a potential

$$V_{\text{sym}} = \frac{1}{2} \gamma_{\text{sym}} \left(\frac{1}{N} \left[\text{Tr}(A_i)^2 \right]_{\text{left}} - \frac{1}{N} \left[\text{Tr}(A_i)^2 \right]_{\text{right}} \right)^2, \quad (\text{A.2})$$

$$\left[\text{Tr}(A_i)^2 \right]_{\text{left}} = \sum_{i=1}^d \sum_{a+b < N+1} |(A_i)_{ab}|^2, \quad (\text{A.3})$$

$$\left[\text{Tr}(A_i)^2 \right]_{\text{right}} = \sum_{i=1}^d \sum_{a+b > N+1} |(A_i)_{ab}|^2, \quad (\text{A.4})$$

where the values of the coefficient γ_{sym} used in our simulation are given in table 2.

To summarize, the model we simulate is given by

$$Z = \int \prod_{a=1}^N d\alpha_a \prod_{i=1}^d dA_i e^{-S_{\text{eff}}}, \quad (\text{A.5})$$

$$S_{\text{eff}} = -2 \log \Delta(\alpha) + V_{\text{pot}} + V_{\text{sym}}.$$

The simulation of the model (A.5) can be performed by using the Hybrid Monte Carlo (HMC) method. First we rewrite the model by introducing auxiliary variables p_a and $(X_i)_{ab}$ ($a, b = 1, \dots, N$) with the action

$$S_{\text{HMC}} = \frac{1}{2} \sum_a (p_a)^2 + \frac{1}{2} \text{Tr}(X_i)^2 + S_{\text{eff}}[\alpha, A]. \quad (\text{A.6})$$

Here p_a are real variables, whereas X_i are traceless Hermitian matrices. We update all the variables in the model (A.6) in the following way. First we regard p_a as the conjugate momenta of α_a and X_i as the conjugate momenta of A_i . Then we regard S_{HMC} in (A.6) as the Hamiltonian H and solve the classical equations of motion obtained as the Hamilton equations

$$\begin{aligned} \frac{d\alpha_a}{d\tau} &= \frac{\partial H}{\partial p_a} = p_a, & \frac{dp_a}{d\tau} &= -\frac{\partial H}{\partial \alpha_a} = -\frac{\partial S_{\text{eff}}}{\partial \alpha_a}, \\ \frac{dA_i}{d\tau} &= \frac{\partial H}{\partial X_i} = X_i^*, & \frac{dX_i}{d\tau} &= -\frac{\partial H}{\partial A_i} = -\frac{\partial S_{\text{eff}}}{\partial A_i}, \end{aligned} \quad (\text{A.7})$$

for some fictitious time τ . This part of the algorithm is called the Molecular Dynamics. In order to solve the Hamilton equations (A.7) numerically, we discretize them using the so-called leap-frog discretization, which maintains reversibility with respect to τ . Starting from the previous configuration at $\tau = 0$, we obtain a new configuration at $\tau = \tau_f$ by solving (A.7) with the step size $\Delta\tau$ so that $\tau_f = N_\tau \cdot \Delta\tau$, where N_τ is the number of steps. We accept the new configuration with the probability $\min(1, \exp(-\Delta S_{\text{HMC}}))$, where

$\Delta S_{\text{HMC}} \equiv S_{\text{HMC}}(\tau_f) - S_{\text{HMC}}(0)$, following the idea of the Metropolis algorithm to satisfy the detailed balance. The important point here is that S_{HMC} is nothing but the Hamiltonian H , which is preserved in the classical dynamics if the equations (A.7) are solved exactly. In fact, ΔS_{HMC} becomes non-zero due to the discretization, but it is guaranteed to be a small quantity of the order of $(\Delta\tau)^2$. By choosing sufficiently small $\Delta\tau$, the acceptance rate can be kept reasonably high, which enables the system to move around efficiently in the configuration space. Note also that the auxiliary variables p_a and $(X_i)_{ab}$ appear only as the Gaussian terms in (A.6). Therefore, we can update them independently by using normalized Gaussian random numbers. This procedure of refreshing the conjugate momenta should be done each time we start a Molecular Dynamics procedure.

To summarize, the HMC algorithm as applied to our system can be described as follows.

1. Generate initial configurations of $p_a(0)$ and $X_i(0)$ with Gaussian distribution $\propto e^{-\frac{1}{2}\sum_a(p_a)^2}$ and $e^{-\frac{1}{2}\text{Tr}(X_i)^2}$, respectively.
2. Evolve the fields $p_a(\tau)$, $X_i(\tau)$, $\alpha_a(\tau)$ and $A_i(\tau)$ for fictitious time τ_f according to the discretized Molecular Dynamics.
3. Accept the configuration of $\alpha_a(\tau_f)$ and $A_i(\tau_f)$ obtained at the end of Molecular Dynamics with the probability $\min(1, e^{-\Delta H})$, where $\Delta H = H(\tau_f) - H(0)$.

In the HMC algorithm, there are two parameters⁷ $\Delta\tau$ and τ_f . In the present work we choose them as in table 2.

N	γ_C/N^2	γ_L/N^2	γ_{sym}	N_τ	$\Delta\tau$	trajectories
128	1	100	200	20	0.0015	2,000,000
256	1	100	200	10	0.0008	1,600,000
384	1	100	2,000	10	0.0004	1,000,000
512	1	100	6,000	10	0.00025	2,250,000

Table 2: The values of the parameters γ_C , γ_L and γ_{sym} in (A.5) used in our simulation. We also give the values of the parameters in the HMC algorithm: the number of steps N_τ in the Molecular Dynamics and its step size $\Delta\tau$. In the last column, we give the number of “trajectories”, which represents how many times we solve the Molecular Dynamics after thermalization to achieve the statistics of our data.

B. Results for the (5+1)D version of the bosonic model

In this section we present our results⁸ for a bosonic model that can be obtained by omitting fermionic matrices in the (5+1)D version of the type IIB matrix model. The latter model is obtained formally by dimensional reducing the 6D $\mathcal{N} = 1$ super Yang-Mills theory to a

⁷These parameters can be optimized as follows. For fixed τ_f , it is optimal to choose $\Delta\tau$ so that $\Delta\tau \times$ (acceptance rate) is maximized. Then τ_f can be optimized to minimize the auto-correlation time in units of one step in the Molecular Dynamics.

⁸Preliminary results shown in Fig. 9 (Right) are published in the proceedings [58].

N	γ_C/N^2	γ_L/N^2	γ_{sym}	N_τ	$\Delta\tau$	trajectories
64	1	100	1,000	10	0.0015	200,000
96	1	100	1,000	10	0.001	400,000
128	1	100	2,000	10	0.001	2,400,000

Table 3: The values of the parameters γ_C , γ_L and γ_{sym} in (A.1) used in our simulation of the (5+1)D model. We also give the values of parameters in the HMC algorithm, (See caption of table 2 for explanation.)

point, and it consists of six bosonic matrices A_μ ($\mu = 1, \dots, 6$) and four fermionic matrices Ψ_α ($\alpha = 1, \dots, 4$) representing four components of a 6D Weyl spinor. The form of the bosonic part of the action is the same as that of the original type IIB matrix model, which is given in (2.2).

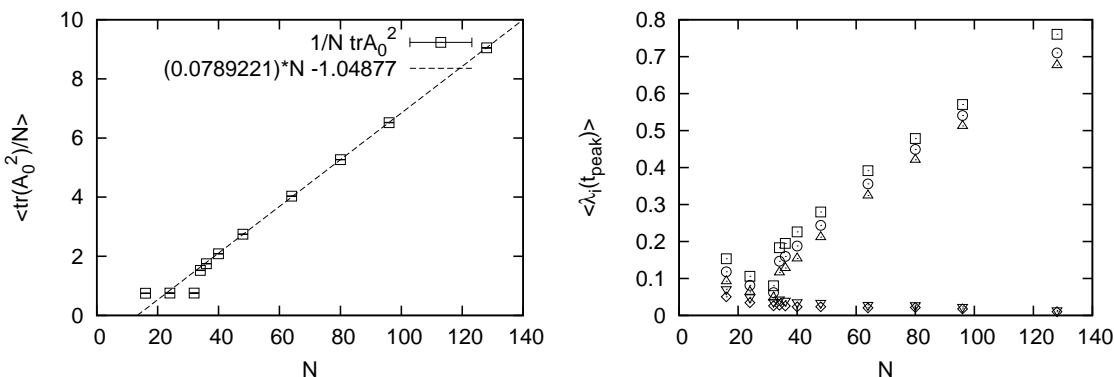


Figure 8: (Left) The extent $\langle \frac{1}{N} \text{Tr}(A_0)^2 \rangle$ of the eigenvalue distribution of A_0 is plotted against N for the (5+1)D model. It starts to increase at $N = N_c = 34$. (Right) The expectation values $\langle \lambda_i(t) \rangle$ of the five eigenvalues of $T_{ij}(t)$ at $t = t_{\text{peak}}$ are plotted against N for the (5+1)D model.

In Fig. 8 (Left), we plot the extent $\langle \frac{1}{N} \text{Tr}(A_0)^2 \rangle$ of the eigenvalue distribution of A_0 against N . In Fig. 8 (Right), we plot the expectation values $\lambda_i(t)$ of the five eigenvalues of $T_{ij}(t)$ at $t = t_{\text{peak}}$ against N . While the qualitative behaviors are the same as in the (9+1)D case shown in Fig. 1, we find that the critical N_c is smaller and the slope of the linearly increasing behavior of $\langle \frac{1}{N} \text{Tr}(A_0)^2 \rangle$ for $N \geq N_c$ is larger. We can understand this difference by considering the attractive potential between the eigenvalues of A_0 discussed below eq. (2.12). For general spatial dimensionality d , one obtains a factor $\Delta^{-2d}(\alpha)$ from integrating out the spatial matrices A_i at one loop. This factor acts as an attractive potential between the eigenvalues of A_0 , and it is stronger for larger d .

Below we discuss the properties of the (5+1)D model for $N \geq N_c$. (The parameters used in the simulation are listed in table 3.) We have determined the block size to be $n = 8, 10, 12$ for $N = 64, 96, 128$, respectively, from the fall-off of the off-diagonal elements of A_i as is done for the (9+1)D case in section 5. In Fig. 9 (Left) we plot the expectation values $\langle \lambda_i(t) \rangle$ of the five eigenvalues of $T_{ij}(t)$ for $N = 128$, which shows that the SO(5)

N	n	t_c	$R(t_c)$	ε	Δ
64	8	-0.7248(5)	0.1575(4)	0.2281(6)	1.825(5)
96	10	-0.7692(3)	0.1276(3)	0.2157(4)	2.157(4)
128	12	-0.8037(1)	0.1070(1)	0.2048(2)	2.457(2)

Table 4: The block size n , the critical time t_c , the extent of space $R(t_c)$ at the critical time, which are used in the (5+1)D model to make the plot in Fig. 9 (Right). We also present the explicit values of the average “lattice spacing” ε and the “volume” Δ in the temporal direction, which are plotted in Fig. 10 (Right).

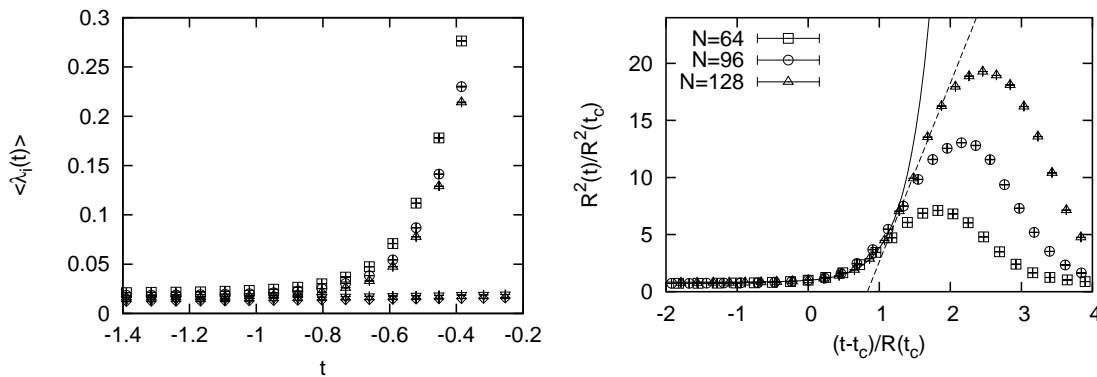


Figure 9: (Left) The expectation values $\langle \lambda_i(t) \rangle$ of the five eigenvalues of $T_{ij}(t)$ are plotted against t for the (5+1)D model with $N = 128$. The critical time is determined as $t_c = -0.8037(1)$. (Right) The extent of space $R^2(t)$ is plotted against $x = (t - t_c)/R(t_c)$ for $N = 64, 96$ and 128 in the (5+1)D model. The solid line represents a fit of the $N = 128$ data to $R^2(t)/R^2(t_c) = a + (1 - a)\exp(bx)$ for $0.4 \leq x \leq 1.2$, which gives $a = 0.839(9)$ and $b = 2.91(6)$. The dashed line represents a fit of the $N = 128$ data to $R^2(t)/R^2(t_c) = cx + d$ for $1.2 \leq x \leq 2.0$, which gives $c = 15.6(5)$ and $d = -13.0(8)$.

symmetry is broken spontaneously down to $SO(3)$ after a critical time. From this kind of figures, we can determine the critical time t_c for each N as described⁹ in section 5.

In Fig. 9 (Right) we show the large- N scaling behavior of the extent of space $R^2(t)$. Explicit values of $R(t_c)$, together with the block size n and the critical time t_c , which are used to make this plot, are given in table 4. The power-law expansion (5.1) is observed at late times similarly to the (9+1)D model.

In Fig. 10 (Left) we plot the t -dependent “lattice spacing”, which shows how the continuum limit is achieved as N increases. The average “lattice spacing” ε and the “volume” Δ in the temporal direction are given in table 4. In Fig. 10 (Right) we plot them in the log scale. The straight lines represent fits to the power-law behaviors.

⁹Unlike in the (9+1)D case, there was no need to adjust the value of t_c to obtain the large- N scaling behavior in Fig. 9 (Right).

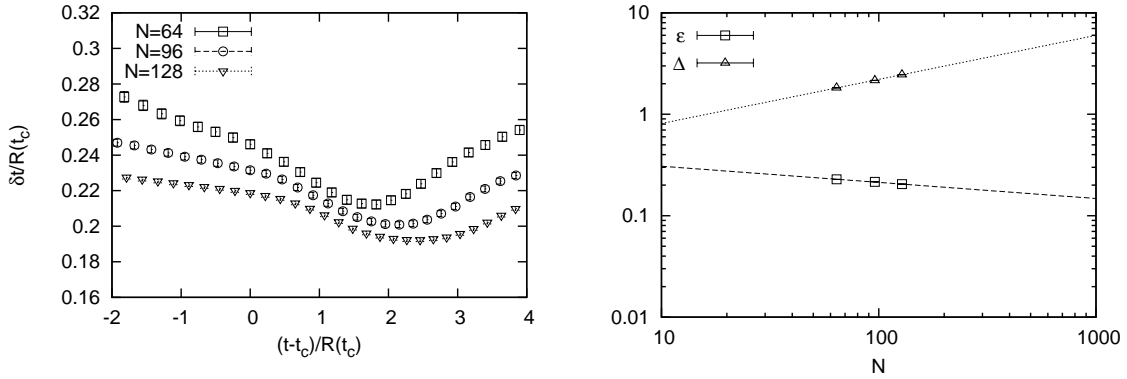


Figure 10: (Left) The “lattice spacing” $\frac{\delta v}{R(t_c)}$ is plotted against $(t - t_c)/R(t_c)$ for the (5+1)D model. (Right) The average “lattice spacing” ϵ and the “volume” in the temporal direction Δ is plotted against N in the log scale for the (5+1)D model. The straight lines represent fits to the power-law behaviors $\epsilon = a N^{-p}$, where $a = 0.44(2)$, $p = 0.16(1)$ and $\Delta = b N^q$, where $b = 0.30(2)$, $q = 0.43(1)$ using all the data.

References

- [1] H. Liu, G. W. Moore and N. Seiberg, *Strings in time dependent orbifolds*, JHEP **0210** (2002) 031 [[hep-th/0206182](#)].
- [2] A. Lawrence, *On the instability of 3-D null singularities*, JHEP **0211** (2002) 019 [[hep-th/0205288](#)].
- [3] G. T. Horowitz and J. Polchinski, *Instability of space - like and null orbifold singularities*, Phys. Rev. D **66** (2002) 103512 [[hep-th/0206228](#)].
- [4] M. Berkooz, B. Craps, D. Kutasov and G. Rajesh, *Comments on cosmological singularities in string theory*, JHEP **0303** (2003) 031 [[hep-th/0212215](#)].
- [5] N. Ishibashi, H. Kawai, Y. Kitazawa and A. Tsuchiya, *A large- N reduced model as superstring*, Nucl. Phys. B, **498** (1997) 467 [[arXiv:hep-th/9612115](#)].
- [6] T. Banks, W. Fischler, S. H. Shenker and L. Susskind, *M theory as a matrix model: a conjecture*, Phys. Rev. D **55** (1997) 5112 [[hep-th/9610043](#)].
- [7] R. Dijkgraaf, E. P. Verlinde and H. L. Verlinde, *Matrix string theory*, Nucl. Phys. B **500** (1997) 43 [[hep-th/9703030](#)].
- [8] P. McFadden and K. Skenderis, *Holography for Cosmology*, Phys. Rev. D **81** (2010) 021301 [[arXiv:0907.5542](#) [[hep-th](#)]].
- [9] A. Bzowski, P. McFadden and K. Skenderis, *Holography for inflation using conformal perturbation theory*, JHEP **1304** (2013) 047 [[arXiv:1211.4550](#) [[hep-th](#)]].
- [10] R. J. Szabo, *Symmetry, gravity and noncommutativity*, Class. Quant. Grav. **23** (2006) R199 [[hep-th/0606233](#)].
- [11] H. Steinacker, *Emergent gravity from noncommutative gauge theory*, JHEP **0712** (2007) 049 [[arXiv:0708.2426](#) [[hep-th](#)]].

- [12] H. Steinacker, *Emergent gravity and noncommutative branes from Yang-Mills matrix models*, Nucl. Phys. B **810** (2009) 1 [arXiv:0806.2032 [hep-th]].
- [13] D. Klammer and H. Steinacker, *Cosmological solutions of emergent noncommutative gravity*, Phys. Rev. Lett. **102** (2009) 221301 [arXiv:0903.0986[gr-qc]].
- [14] H. Steinacker, *Emergent geometry and gravity from matrix models: an introduction* Class. Quant. Grav. **27** (2010) 133001 [arXiv:1003.4134[hep-th]].
- [15] H. S. Yang, *Emergent gravity from noncommutative spacetime* Int. J. Mod. Phys. A **24** (2009) 4473 [hep-th/0611174].
- [16] H. S. Yang, *Emergent spacetime and the origin of gravity* JHEP **0905** (2009) 012 [arXiv:0809.4728 [hep-th]].
- [17] H. S. Yang, *Emergent spacetime and cosmic inflation*, arXiv:1503.00712 [hep-th].
- [18] H. Aoki, N. Ishibashi, S. Iso, H. Kawai, Y. Kitazawa and T. Tada, *Noncommutative Yang-Mills in IIB matrix model*, Nucl. Phys. B **565** (2000) 176 [hep-th/9908141].
- [19] J. Ambjorn, Y. M. Makeenko, J. Nishimura and R. J. Szabo, *Finite N matrix models of noncommutative gauge theory*, JHEP **9911** (1999) 029 [hep-th/9911041].
- [20] J. Ambjorn, Y. M. Makeenko, J. Nishimura and R. J. Szabo, *Nonperturbative dynamics of noncommutative gauge theory*, Phys. Lett. B **480** (2000) 399 [hep-th/0002158].
- [21] J. Ambjorn, Y. M. Makeenko, J. Nishimura and R. J. Szabo, *Lattice gauge fields and discrete noncommutative Yang-Mills theory*, JHEP **0005** (2000) 023 [hep-th/0004147].
- [22] G. Ishiki, *Matrix geometry and coherent states* arXiv:1503.01230 [hep-th].
- [23] M. H. de Bady, J. L. Karczmarek, P. Sabella-Garnier and K. H. C. Yeh, *Emergent geometry of membranes*, arXiv:1506.02035 [hep-th].
- [24] M. Hanada, H. Kawai and Y. Kimura, *Describing curved spaces by matrices*, Prog. Theor. Phys. **114** (2006) 1295 [hep-th/0508211].
- [25] H. Aoki, S. Iso, H. Kawai, Y. Kitazawa and T. Tada, *Space-time structures from IIB matrix model*, Prog. Theor. Phys. **99** (1998) 713 [hep-th/9802085].
- [26] T. Hotta, J. Nishimura and A. Tsuchiya, *Dynamical aspects of large N reduced models*, Nucl. Phys. B **545** (1999) 543 [hep-th/9811220].
- [27] J. Ambjorn, K. N. Anagnostopoulos, W. Bietenholz, T. Hotta and J. Nishimura, *Large N dynamics of dimensionally reduced 4D $SU(N)$ superYang-Mills theory*, JHEP **0007** (2000) 013 [hep-th/0003208].
- [28] J. Ambjorn, K. N. Anagnostopoulos, W. Bietenholz, T. Hotta and J. Nishimura, *Monte Carlo studies of the IIB matrix model at large N* , JHEP **0007** (2000) 011 [hep-th/0005147].
- [29] K. N. Anagnostopoulos and J. Nishimura, *New approach to the complex action problem and its application to a nonperturbative study of superstring theory*, Phys. Rev. D **66** (2002) 106008 [hep-th/0108041].
- [30] J. Nishimura and G. Vernizzi, *Spontaneous breakdown of Lorentz invariance in IIB matrix model*, JHEP **0004** (2000) 015 [hep-th/0003223].
- [31] J. Nishimura and G. Vernizzi, *Brane world from IIB matrices*, Phys. Rev. Lett. **85** (2000) 4664 [hep-th/0007022].

- [32] J. Nishimura and F. Sugino, *Dynamical generation of four-dimensional space-time in the IIB matrix model*, JHEP **0205** (2002) 001 [[hep-th/0111102](#)].
- [33] H. Kawai, S. Kawamoto, T. Kuroki, T. Matsuo and S. Shinohara, *Mean field approximation of IIB matrix model and emergence of four-dimensional space-time*, Nucl. Phys. B **647** (2002) 153 [[hep-th/0204240](#)].
- [34] T. Aoyama and H. Kawai, *Higher order terms of improved mean field approximation for IIB matrix model and emergence of four-dimensional space-time*, Prog. Theor. Phys. **116** (2006) 405 [[hep-th/0603146](#)].
- [35] T. Imai, Y. Kitazawa, Y. Takayama and D. Tomino, *Quantum corrections on fuzzy sphere*, Nucl. Phys. B **665** (2003) 520 [[hep-th/0303120](#)].
- [36] T. Imai, Y. Kitazawa, Y. Takayama and D. Tomino, *Effective actions of matrix models on homogeneous spaces*, Nucl. Phys. B **679** (2004) 143 [[hep-th/0307007](#)].
- [37] T. Imai and Y. Takayama, *Stability of fuzzy $S^2 \times S^2$ geometry in IIB matrix model*, Nucl. Phys. B **686** (2004) 248 [[hep-th/0312241](#)].
- [38] K. N. Anagnostopoulos, T. Azuma and J. Nishimura, *Monte Carlo studies of the spontaneous rotational symmetry breaking in dimensionally reduced super Yang-Mills models*, JHEP **1311** (2013) 009 [[arXiv:1306.6135](#) [[hep-th](#)]].
- [39] W. Krauth, H. Nicolai and M. Staudacher, *Monte Carlo approach to M theory*, Phys. Lett. B **431**(1998) 31 [[hep-th/9803117](#)].
- [40] P. Austing and J. F. Wheeler, *Convergent Yang-Mills matrix theories*, JHEP **0104** (2001) 019 [[hep-th/0103159](#)].
- [41] J. Ambjorn, J. Jurkiewicz and R. Loll, *Reconstructing the universe*, Phys. Rev. D **72** (2005) 064014 [[hep-th/0505154](#)].
- [42] H. Kawai and T. Okada, *Asymptotically vanishing cosmological constant in the multiverse*, Int. J. Mod. Phys. A **26** (2011) 3107 [[arXiv:1104.1764](#) [[hep-th](#)]].
- [43] J. Nishimura, T. Okubo and F. Sugino, *Systematic study of the $SO(10)$ symmetry breaking vacua in the matrix model for type IIB superstrings*, JHEP **1110** (2011) 135 [[arXiv:1108.1293](#) [[hep-th](#)]].
- [44] S. W. Kim, J. Nishimura and A. Tsuchiya, *Expanding (3+1)-dimensional universe from a Lorentzian matrix model for superstring theory in (9+1)-dimensions*, Phys. Rev. Lett. **108** (2012) 011601 [[arXiv:1108.1540](#) [[hep-th](#)]].
- [45] S. W. Kim, J. Nishimura and A. Tsuchiya, *Expanding universe as a classical solution in the Lorentzian matrix model for nonperturbative superstring theory*, Phys. Rev. D **86** (2012) 027901 [[arXiv:1110.4803](#) [[hep-th](#)]].
- [46] S. W. Kim, J. Nishimura and A. Tsuchiya, *Late time behaviors of the expanding universe in the IIB matrix model* JHEP **1210** (2012) 147 [[arXiv:1208.0711](#) [[hep-th](#)]].
- [47] A. Stern, *Matrix model cosmology in two space-time dimensions*, Phys. Rev. D **90** (2014) 12, 124056 [[arXiv:1409.7833](#) [[hep-th](#)]].
- [48] A. Chatzistavrakidis, *Dynamical phase space from a $SO(d, d)$ matrix model*, Phys. Rev. D **90** (2014) 12, 121502 [[arXiv:1407.7054](#) [[hep-th](#)]].
- [49] A. Chaney, Lei Lu, A. Stern, *Lorentzian fuzzy spheres*, [arXiv:1506.03505](#) [[hep-th](#)].

- [50] J. Nishimura and A. Tsuchiya, *Local field theory from the expanding universe at late times in the IIB matrix model*, PTEP **2013** (2013) 043B03. [[arXiv:1208.4910](#) [[hep-th](#)]].
- [51] A. Chatzistavrakidis, H. Steinacker and G. Zoupanos, *Intersecting branes and a standard model realization in matrix models*, JHEP **1109** (2011) 115 [[arXiv:1107.0265](#) [[hep-th](#)]].
- [52] H. Aoki, *Chiral fermions and the standard model from the matrix model compactified on a torus*, Prog. Theor. Phys. **125** (2011) 521 [[arXiv:1011.1015](#) [[hep-th](#)]].
- [53] J. Nishimura and A. Tsuchiya, *Realizing chiral fermions in the type IIB matrix model at finite N* , JHEP **1312** (2013) 002 [[arXiv:1305.5547](#) [[hep-th](#)]].
- [54] H. C. Steinacker and J. Zahn, *An extended standard model and its Higgs geometry from the matrix model*, PTEP **2014** (2014) 8, 083B03 [[arXiv:1401.2020](#) [[hep-th](#)]].
- [55] H. Aoki, J. Nishimura and A. Tsuchiya, *Realizing three generations of the Standard Model fermions in the type IIB matrix model*, JHEP **1405** (2014) 131 [[arXiv:1401.7848](#) [[hep-th](#)]].
- [56] H. C. Steinacker, *Spinning squashed extra dimensions and chiral gauge theory from $N=4$ SYM*, Nucl. Phys. B **896** (2015) 212 [[arXiv:1411.3139](#) [[hep-th](#)]].
- [57] Y. Ito, S. W. Kim, Y. Koizuka, J. Nishimura and A. Tsuchiya, *A renormalization group method for studying the early universe in the Lorentzian IIB matrix model*, PTEP **2014** (2014) 083B01 [[arXiv:1312.5415](#) [[hep-th](#)]].
- [58] Y. Ito, S. W. Kim, J. Nishimura and A. Tsuchiya, *Monte Carlo studies on the expanding behavior of the early universe in the Lorentzian type IIB matrix model*, PoS LATTICE **2013** (2014) 341 [[arXiv:1311.5579](#) [[hep-lat](#)]].